

NJC

Accepted Manuscript



This is an *Accepted Manuscript*, which has been through the Royal Society of Chemistry peer review process and has been accepted for publication.

Accepted Manuscripts are published online shortly after acceptance, before technical editing, formatting and proof reading. Using this free service, authors can make their results available to the community, in citable form, before we publish the edited article. We will replace this *Accepted Manuscript* with the edited and formatted *Advance Article* as soon as it is available.

You can find more information about *Accepted Manuscripts* in the [Information for Authors](#).

Please note that technical editing may introduce minor changes to the text and/or graphics, which may alter content. The journal's standard [Terms & Conditions](#) and the [Ethical guidelines](#) still apply. In no event shall the Royal Society of Chemistry be held responsible for any errors or omissions in this *Accepted Manuscript* or any consequences arising from the use of any information it contains.



www.rsc.org/njc

Cite this: DOI: 10.1039/c0xx00000x

www.rsc.org/xxxxxx

ARTICLE TYPE**Morphology-controlled synthesis of large mordenite crystals**

Yaming Mao, Yu Zhou, Haimeng Wen, Jingyan Xie, Wei Zhang, Jun Wang*

Received (in XXX, XXX) Xth XXXXXXXXXX 20XX, Accepted Xth XXXXXXXXXX 20XX

DOI: 10.1039/b000000x

The morphology-controlled synthesis of mordenite (MOR) zeolite was achieved using the acidic hydrolysis route, which was started by acid-catalyzed hydrolysis of tetraethylorthosilicate (TEOS), followed by switching the synthetic gel to basic condition for hydrothermal crystallization. The synthesis by using tetraethylammonium hydroxide as the template resulted in a series of large MOR crystals with different morphologies, such as bulky sphere, circular pie, flat prism, hexagonal star-like prism and ellipsoid. Moreover, column, elongated spindle, short spindle, petal and circular pie shaped MOR crystals could be obtained without using organic template in the above synthetic route. Among these morphologies, the bulky sphere, hexagonal star-like prism and petal shaped crystals were generated on MOR zeolites for the first time. The obtained products were characterized by XRD, SEM and N₂ adsorption experiments. Various synthetic parameters were systematically investigated, including hydrolysis condition of TEOS, molar composition of initial gel, crystallization time and temperature. The results demonstrated that MOR zeolite can be synthesized through the acidic hydrolysis route, and their morphology can be facilely controlled through tuning elemental synthetic conditions.

Keywords: zeolite; mordenite; morphology control; hydrothermal synthesis; crystal

1. Introduction

Zeolites are crystalline aluminosilicates with well-defined microporous structures^[1-2]. The ordered frameworks and specific pore/channel structures of zeolites make them to be widely applied as adsorbents, detergents, ion-exchangers, and heterogeneous catalysts^[2,3]. The morphology control of zeolites is important both for fundamental research and industrial applications because the shape and size of zeolites significantly affect their performances^[3-5]. For instance, microspheres are attractive in separation processes^[6,7]. The uniform clustered NaY zeolite microspheres (5 μm) with rugged surface were highly selective in removal of tobacco specific nitrosamine carcinogens^[8]. The formation of zeolite morphology is sensitive to synthetic conditions, therefore it is essential to investigate synthetic parameters that affect the crystal size and shape^[9-11]. It is still a challenge to fabricate suitable morphology on required zeolites due to the complicate relationship between zeolite morphologies and synthetic conditions.

Among hundreds of structures for zeolite frameworks, mordenite (framework MOR) has found practical applications, especially in alkylation, hydroisomerization, reforming, dewaxing and cracking processes^[12-14]. In 1864, How^[15] firstly described that mordenite had chemical formula Na₈(H₂O)₂₄[Si₄₀Al₈O₉₆] and parallel 12-membered ring (MR) channels (0.67 × 0.70 nm) along c-axis direction, which were interconnected by 8-MR (0.34 × 0.48 nm) along b-axis direction with the *Cmcm* space group^[16-17]. So far, MOR samples with different morphologies, such as rod, needle, disk, column, sphere and prism, have been successfully synthesized. For example, Sharma *et al.* synthesized nanosized mordenite analogues with spherical shape using low

concentration of NaOH^[18]. Zhou *et al.* reported the hydrothermal synthesis of mordenite membrane in fluoride media on porous tubular mullite supports, and the obtained material exhibited global polycrystalline morphology with the average size of approximately 1.0 μm^[19]. Although mordenite crystals with spherical morphology have been reported, the sizes of these mordenite spheres were below 1 μm. Zeolites with microspherical morphology have the advantages of easy handling, limited attrition and convenient recycling in catalytic applications^[20], as well as the potential candidates in chromatographic separation^[21-23]. So, it is desirable to develop new route to control the morphology of mordenite, especially to synthesize bulky spherical mordenite.

Silica source is one of the most significant factors in zeolite synthesis, because it can largely influence the morphology and crystal size of zeolite^[24]. Sodium metasilicate, colloidal silica, fumed silica, water glass and tetraethylorthosilicate (TEOS) have been used for the synthesis of mordenite^[18]. When TEOS is hydrolyzed in acidic condition, the produced silica precursors are different from those in basic condition^[25], which my favour the morphology control of zeolite^[26]. Recently, our group found that zeolite MCM-22, ZSM-5 and Beta could be obtained by acid-catalyzed hydrolysis of TEOS^[26-29]; however, the synthesis of mordenite via the acidic hydrolysis of TEOS has not been reported.

In this study, we report the morphology-controlled synthesis of MOR zeolite through the acidic hydrolysis of TEOS. Large mordenite crystals with various morphologies (bulky sphere, circular pie, flat prism, hexagonal star-like prism, ellipsoid, column, elongated spindle, short spindle and petal) are synthesized merely by changing the elemental synthetic conditions, such as the initial gel compositions and crystallization

temperature/time. Among them, the bulky sphere, hexagonal star-like prism and petal shaped crystals are firstly generated on MOR zeolite to the best of our knowledge. The influence of various synthetic parameters is systematically investigated in order to explore the formation regulation of the morphologies.

2. Experimental section

2.1. Synthesis

The mordenite zeolites were synthesized through a hydrothermal route. The typical procedure was as follows. A total of 6.34 g TEOS (28.4 wt. % SiO₂, Sinopharm Chem. Reagent Co., AR) was mixed with 10 g deionized water in an open glass beaker. Under vigorous stirring, the concentrated hydrochloric acid (Shanghai Chem. Reagent Co., AR) was slowly dropped into the TEOS solution to obtain a pH value of 1.0. The obtained mixture A was stirred at 293 K for 24 h to get a complete hydrolysis of TEOS. 2.21 g tetraethylammonium hydroxide (TEAOH) (35 wt.% aqueous solution, Jintan Huadong Chem. Res. Institute, AR), 1.35 g Al₂(SO₄)₃·18 H₂O, 1.00 g NaOH and 20 g deionized water were mixed together to get solution B. Afterwards, solutions A and B were mixed at room temperature and stirred for 10 min. The obtained slurry was aged at room temperature for 24 h. Finally, the slurry was transferred to a Teflon-lined stainless steel autoclave and left to crystallize statically at 443 K. The final composition of the gel was 15SiO₂/8Na₂O/900H₂O/3.5TEAOH/1Al₂O₃. The solid was separated by filtration, washed with deionized water and air-dried at 373 K. The obtained as-synthesized sample was calcined at 823 K to remove the template. Other samples were synthesized similarly but with different compositions of the initial gels and crystallization conditions, as seen in Table 1. For convenient descriptions, sample names were designated with the Entries in Table 1.

For comparison, the base-hydrolysis sample was prepared following the same procedure, except that the silica precursor was prepared by catalytically hydrolyzing TEOS in the NaOH medium (instead of HCl) at pH = 10.

2.2. Characterization

X-ray diffraction (XRD) patterns were collected on the Bruker D8 ADVANCE powder diffractometer equipped with Ni-filtered Cu K α radiation source at 45 kV and 200 mA, from 5° to 50° with a scan rate of 0.2°/s. The Brunauer-Emmett-Teller (BET) surface areas were measured at the temperature of liquid nitrogen using a Micromeritics ASAP2010 analyzer, and the samples were degassed at 573 K to a vacuum of 10⁻³ Torr before analysis. The Si to Al molar ratio of final solid was obtained using ADVANT'XP X-ray fluorescence spectroscopy (ThermoFisher Scientific). Scanning electron microscope (SEM) images were recorded on an environmental scanning electron microscope (Quanta 200, FEI).

3. Results

3.1. Effect of Na₂O/SiO₂/Al₂O₃ ratio

Figure 1A shows the XRD patterns of the products synthesized with the initial gel composition of SiO₂/Na₂O/H₂O/TEAOH = 15/8.0/900/3.50 (crystallized at 443 K for 96 h) by varying the aluminum contents to be $n = 10, 15, 20, 30$ and 40 (n : molar ratio

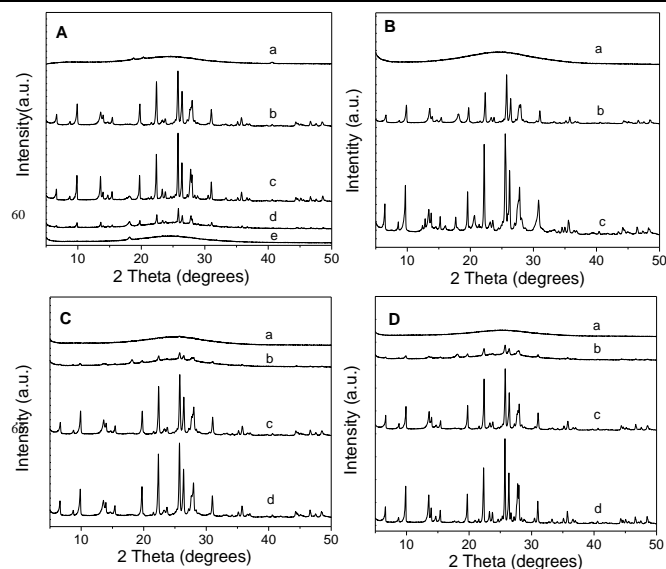


Figure 1. XRD patterns of as-calcined MOR samples obtained under different conditions (A) SiO₂/Al₂O₃ molar ratio (a = 10, b = 15, c = 20, d = 30, e = 40); (B) Na₂O/Al₂O₃ molar ratio (a = 7.0, b = 8.5, c = 9.0); (C) crystallization time (a = 1 d, b = 2 d, c = 3 d, d = 5 d); (D) crystallization temperature (a = 423 K, b = 433 K, c = 453 K, d = 473 K).

of SiO₂ to Al₂O₃ in initial gels). Only amorphous solid forms in the case of concentrated aluminum content ($n = 10$), while highly crystallized MOR samples are obtained in the case of suitable aluminum contents (Entries 1 and 2 at $n = 15$ and 20 respectively, Table 1). Decreasing of the aluminum content to $n = 30$ can still produce MOR zeolite (Entry 3), but the XRD intensity (curve d, Figure 1A) becomes weaker, reflecting a lower crystallinity. Further decreasing the aluminum content to $n = 40$, the XRD result (curve e, Figure 1A) displays an amorphous structure for the obtained solid. The final SiO₂ to Al₂O₃ molar ratios of solid products are 14, 16 and 19 for Entries 1-3 respectively, which are slightly smaller than those in initial gels. Therefore, an increase of the aluminum in initial gels lead to more aluminum incorporated in the final MOR solids.

The SEM images of the above three MOR zeolites are shown in Figure 2. The sample at $n = 15$ (Entry 1) displays a spherical morphology with the diameter of ca. 40 μm . The high-magnification view (inset of Figure 2A) shows that these bulky spheres are aggregated with the small-sized strip-like crystals (500–800 nm), which may contribute to the broadening phenomenon of the XRD peaks (curve b, Figure 1A). Moreover, the inside of these bulky spheres (Figure S1) are also the assembly of the small-sized strip-shaped crystals. To the best of our knowledge, this morphology has never been reported on MOR zeolite so far. With the increase of SiO₂/Al₂O₃, the morphology changes from bulky sphere ($n = 15$, Figure 2A) to circular pie with size of 40×20 μm for the sample Entry 2 ($n = 20$, Figure 2B) and then to flat prism with size of 40×10 μm for the sample Entry 3 ($n = 30$, Figure 2C). Lowenstein's rule^[30] has described morphology variation where aluminum species can only connect with silicon species whereas silicon species can link either silicon or aluminum. It seems suggested that the small primary crystals fabricating the bulky spheres is relative to the low SiO₂/Al₂O₃ ratio, in agreement with the previous observation

Table 1 Synthesis conditions and textural properties of MOR zeolite

Sample	Synthetic conditions		Textural properties		
	SiO ₂ /Na ₂ O/H ₂ O/TEAOH/Al ₂ O ₃ ^a	Crystallization condition	Morphology ^b	Dimensions ^c (ca. μm)	SiO ₂ /Al ₂ O ₃ ^d (mol mol ⁻¹)
Entry 1	15/8.0/900/3.50/1	443 K, 96 h	Sphere	40 × 40	14.05
Entry 2	15/8.0/900/3.50/0.75	443 K, 96 h	Circular pie	40 × 20	15.92
Entry 3	15/8.0/900/3.50/0.5	443 K, 96 h	Flat prism	40 × 10	19.39
Entry 4	15/8.5/900/3.50/1	443 K, 96 h	Circular pie	20 × 10	13.73
Entry 5	15/8.0/900/3.50/1	443 K, 48 h	Sphere	40 × 40	15.97
Entry 6	15/8.0/900/3.50/1	443 K, 72 h	Sphere	40 × 40	16.17
Entry 7	15/8.0/900/3.50/1	453 K, 96 h	Sphere	50 × 50	12.07
Entry 8	15/8.0/900/3.50/1	473 K, 96 h	Hexagonal star-like prism	45 × 45	11.78
Entry 9	15/8.0/800/3.50/1	443 K, 96 h	Circular pie	40 × 20	17.00
Entry 10	15/8.0/850/3.50/1	443 K, 96 h	Ellipsoid	40 × 30	14.50
Entry 11	15/8.3/900/2.00/1	443 K, 96 h	Sphere	40 × 40	17.00
Entry 12	15/9.0/900/0.00/1	443 K, 96 h	Column	25 × 20	8.97
Entry 13	20/8.0/900/0.00/1	443 K, 96 h	Elongated spindle	70 × 30	16.13
Entry 14	20/9.0/900/0.00/1	443 K, 96 h	Short spindle	50 × 35	15.89
Entry 15	15/8.0/480/0.00/1	443 K, 96 h	Petal	60 × 50	14.37
Entry 16	15/10.0/900/0.00/1	443 K, 96 h	Circular pie	30 × 20	13.72

^a The molar ratio of different component in the gel;

^b The morphologies of the mordenite crystals are obtained from SEM images;

^c The dimensions of the mordenite crystals are obtained from SEM images;

^d The SiO₂ to Al₂O₃ molar ratios for the final solid products analyzed by XRF.

that an Al-rich system could accelerate the nucleation and growth processes causing the creation of zeolitic nanocrystallites^[31].

If TEOS is hydrolyzed in basic rather than acidic condition, the obtained sample still displays pure MOR phase according to the XRD pattern (Figure S2). Nonetheless, its SEM image (Figure S3) shows that they are circular pie-shaped particles with the size of ca. 40 μm. The comparison suggests that the acidic hydrolysis route should have played a key role in the formation of the unusual sphere morphology, consistent with our previous results for ZSM-5 and β zeolite^[26,28]. For hydrolysis of TEOS, it has been demonstrated that silica precursors obtained under acid-catalyzed conditions are highly overlapped or entangled, whereas under basic conditions, they are interpenetrated and behave as discrete clusters^[32]. Similarly, Sanchez *et al.*^[33] and Sefcik *et al.*^[34] revealed that the rate-limiting steps under acidic and basic conditions were condensation and hydrolysis, respectively, and the former caused small cage-like units, while later generated larger silicate particles. Also, our previous work^[27] showed much smaller silicate colloidal (100~200 nm) with acid hydrolysis of TEOS than those (500~800 nm) at base conditions. The above considerations allow to suggest that the small-sized MOR crystals from acid hydrolysis route here may relate to the smaller silicate precursors; however, to confirm this still needs more evidence.

Figure 1B shows the XRD patterns for the samples obtained with different alkalinities using the initial gel compositions of SiO₂/Na₂O/H₂O/TEAOH/Al₂O₃ = 15/y/900/3.50/1 (y denotes the molar ratio of Na₂O to Al₂O₃) with crystallization at 443 K for 96 h. It can be seen that no crystalline phase forms when the alkalinity is too low at y = 7.0 (curve a, Figure 1B). Increasing the alkalinity up to y = 8.5 can generate pure MOR phase, and the crystal shape changes from bulky sphere (y = 8, Figure 2A) to

circular pie (y = 8.5, Figure 2D). These circular pie-shaped crystals have the diameter of ca. 20 μm, much smaller than that of the sample Entry 2 with the size of ca. 40 μm (Table 1). The decrease of the crystal size may be due to the restriction of the polycondensation of hydroxoaluminate and the silicate ions in higher alkalinity^[35]. At y = 9.0, only the mixed phase of MOR with hydroxysodalite forms (Figure S4), and the product morphology shows small spherical particles embedded in the surface of the mordenite bulky sphere sized at 40 μm (Figure S5). These small spherical particles are hydroxysodalite crystals looking like balls of yarn with a particle size ca. 10 μm.

3.2. Effect of crystallization conditions

The formation procedure of the bulky spheres is studied by changing the crystallization time. Before onset of hydrothermal crystallization, only irregular fragments are observed (Figure 2E). One day crystallization causes a few cauliflower-like aggregates with sizes ca. 20 μm surrounded by a large amount of particles (Figure 2F), and these aggregates are still amorphous, confirmed by the XRD patterns of Figure 1C. When the crystallization time exceeds 2 days, the weak characteristic diffraction peaks for MOR appear, suggesting a semi-amorphous structure with sizes ca. 40 μm, as illustrated by the SEM image of Figure 2G. It seems that the semi-amorphous particles at this early growing stage are composed of small-sized incomplete crystalline units, indicating that the bulky spheres are assembled by nanocrystallines. Higher crystallinity can be achieved as the time is up to 3 days. The formed spherical particles are aggregated by small-sized primary crystals and have smooth surface (Figure 2H). Further increasing the crystallization time to 4 days (Figure 2A) results in regular bulky spheres with thicker and larger primary

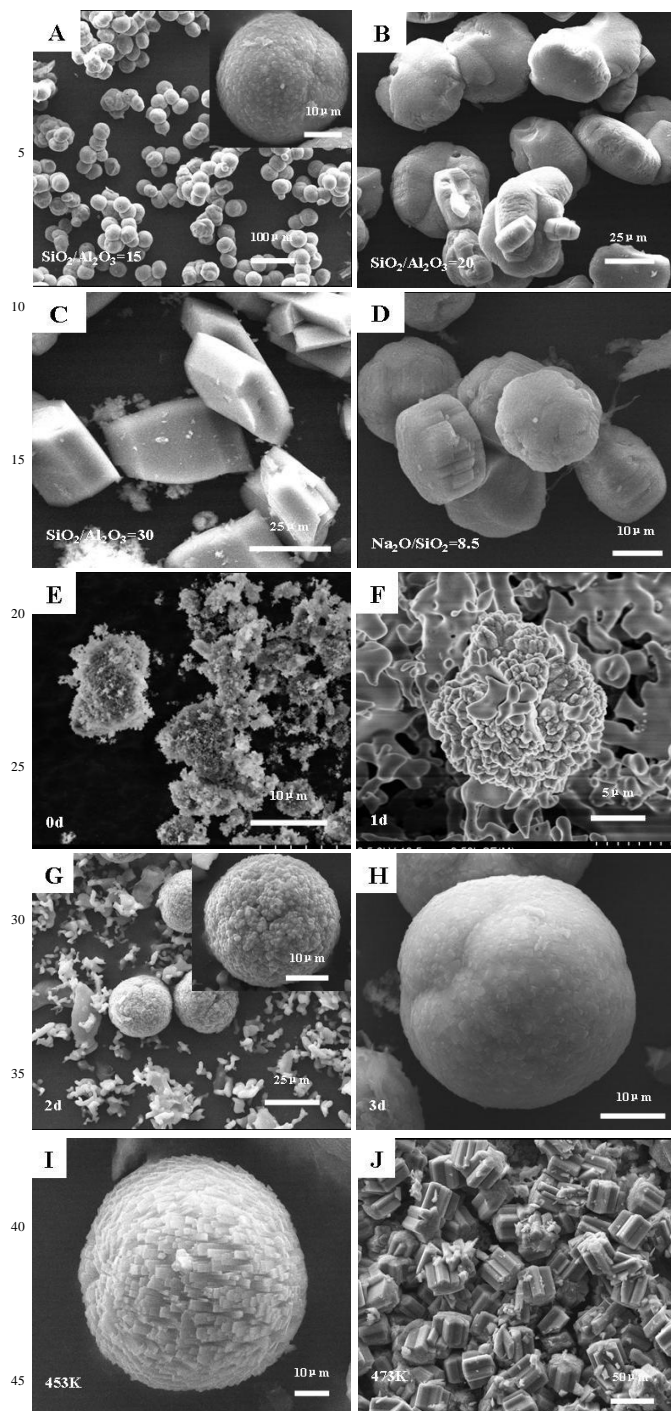


Figure 2. SEM images of MOR samples obtained by varying $\text{SiO}_2/\text{Al}_2\text{O}_3$ or $\text{Na}_2\text{O}/\text{SiO}_2$ ratios (A: Entry 1; B: Entry 2; C: Entry 3; D: Entry 4), and crystallization conditions (G: Entry 5; H: Entry 6; I: Entry 7; J: Entry 8).

crystals, and the edges/corners of the primary crystals become apparent. At the same time, the amorphous species around the bulky spheres are consumed during the crystallization process. The nitrogen sorption isotherm of the sample (Figure S8a) exhibits high nitrogen uptakes at low relative pressures ($p/p_0 < 0.1$) with BET surface area of $405 \text{ m}^2 \text{ g}^{-1}$ and pore volume of $0.21 \text{ cm}^3 \text{ g}^{-1}$ (Table S1). When the crystallization time increases to 9

60 days, it is still pure MOR phase (Figure S6) exhibiting unchanged morphology (Figure S7).

It is well established that the crystallization temperature significantly influences the nucleation and crystal growth in the synthesis of zeolite [36]. Figure 1D shows the XRD patterns of the samples obtained at different crystallization temperatures. The crystallinity of zeolite MOR increases with raising the temperature from 423 K to 473 K. At 423 K, only amorphous phase is observed (curve a, Figure 1D). When the temperature is 433 K, the diffraction peaks for MOR structure appears, which is accompanied with amorphous phase featured by a very broad peak at $20\text{--}30^\circ$ (curve b, Figure 1D). A higher crystallinity for the sample Entry 1 is achieved when the temperature increases to 443 K (curve b, Figure 1A). The morphology of sample Entry 7 synthesized at 453 K (Figure 2J) is similar to the one obtained at 443 K, except that the size of the primary crystals in the former is larger than that in the later. This may be attributed to that the higher temperature can accelerate the solubility of silicate species, leading to the rapid growth of crystal nucleus [37]. At the highest temperature 473 K, the obtained sample Entry 8 presents a new morphology (Figure 2J) that has not been reported before: the primary particles are square prisms and parallel aligned to form hexagonal star-like bundles sized at ca $45 \mu\text{m}$. The nitrogen sorption isotherm of the sample Entry 8 is shown in Figure S8b, giving BET surface area and pore volume of $387 \text{ m}^2 \text{ g}^{-1}$ and $0.20 \text{ cm}^3 \text{ g}^{-1}$, respectively (Table S1).

3.3. Effect of water amount

In hydrothermal synthesis, water not only provides an indispensable medium for the dissolution and diffusion of aluminosilicate, but also determines the concentration and viscosity of the synthesis gel [38]. Figure 3A displays the XRD patterns of the samples synthesized with the gel compositions of $\text{SiO}_2/\text{Na}_2\text{O}/\text{H}_2\text{O}/\text{TEAOH}/\text{Al}_2\text{O}_3 = 15/8/z/3.50/1$ (z denotes the molar ratio of H_2O to Al_2O_3). SEM images of the selected samples (Entries 9 and 10) are shown in Figure 4. When $\text{H}_2\text{O}/\text{Al}_2\text{O}_3$ ratio is 800, the sample Entry 9 is pure MOR phase (curve a, Figure 3A). The morphology of sample Entry 9 (Figure 4A) is circular pie with sizes ca. $40 \mu\text{m}$. The higher magnification image (inset of Figure 4A) shows the well crystallized primary crystals (500 nm) with the rectangular-sheet shape on the edge of the circular pie, and the primary crystals are packed layer by layer in a large degree of confusion. With the water amount increased to $z = 850$, the circular pie crystals swells and evolves to ellipsoid

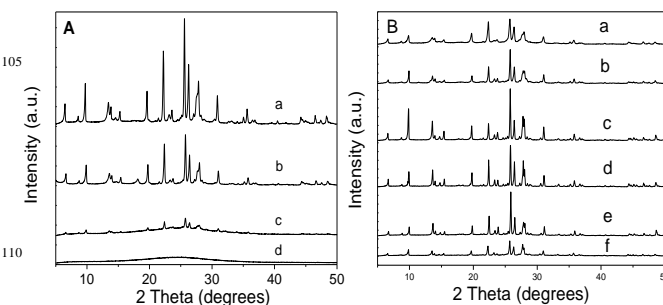


Figure 3. XRD patterns of as-calcined MOR samples obtained with the crystallization time of 4 d, crystallization temperature of 443 K and different gel compositions. (A) gel composition $15\text{SiO}_2/8\text{Na}_2\text{O}/3.5\text{TEAOH}/1\text{Al}_2\text{O}_3$ with $\text{H}_2\text{O}/\text{Al}_2\text{O}_3$ molar ratios of (a) = 800, (b) = 850, (c) = 950, (d) = 1000; (B) gel composition $x\text{SiO}_2/y\text{Na}_2\text{O}/z\text{H}_2\text{O}/m\text{TEAOH}/1\text{Al}_2\text{O}_3$: (a) $x = 15$, $y = 8.3$, $z = 900$, $m = 2$; (b) $x = 15$, $y = 9$, $z = 900$, $m = 0$; (c) $x = 20$, $y = 8$, $z = 900$, $m = 0$; (d) $x = 20$, $y = 9$, $z = 900$, $m = 0$; (e) $x = 15$, $y = 8$, $z = 480$, $m = 0$; (f) $x = 15$, $y = 10$, $z = 900$, $m = 0$.

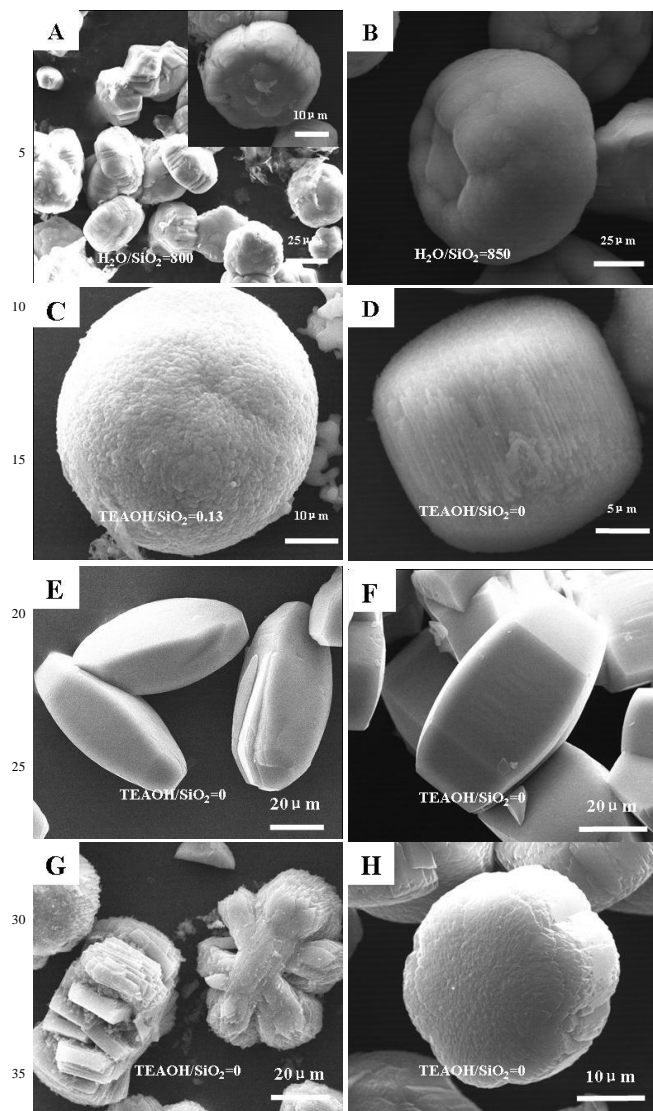


Figure 4. SEM images of MOR samples obtained with the crystallization time of 4 d, crystallization temperature of 443 K and other different conditions (A Entry 9 and B Entry 10): different $\text{H}_2\text{O}/\text{Al}_2\text{O}_3$ ratios; (C Entry 11): low TEAOH amount; (D Entry 12, E Entry 13, F Entry 14, G Entry 15, H Entry 16): template-free synthesized samples.

(Entry 10, Figure 4B). The primary particles of the ellipsoid are strip-like shaped small-sized crystals, similar to the building units of the bulky sphere (Entry 1). When $z = 900$, the ellipsoid shaped crystals keep swelling up and finally turn to spherical micro-sized particles (Entry 1). Furthermore, it can be seen from the SEM images (Figures 2A, 4A and 4B) that the sizes of the building units of these aggregations become smaller as the water amount increases, and the crystals habit of these building units change gradually with an increased c/b (a) aspect ratio, indicating that a diluted gel benefits a preferential growth along the c direction. The framework density of the a - b plane is lower than the c direction, so slower growth would benefit the growth of the higher density facets^[39]. As a consequence, strip-like small-sized crystals with c -elongation that assemble the mordenite bulky spheres are formed gradually in diluted systems. Moreover, formation of aggregated bulky spheres stabilizes those small-sized crystals by decreasing the surface energy^[26]. When the

water amount increases to $z = 950$, the obtained material still presents MOR phase but with a weak intensity of XRD peak, indicating appearance of amorphous phase (curve c, Figure 3A).

Increasing the water amount to $z = 1000$ only leads to an amorphous phase (curve d, Figure 3A).

3.4. Effect of TEAOH amount

Organic templates not only play significant roles in zeolite nucleation and growth due to their capability in altering gel chemistry^[40] and directing typical oligomers into a specific framework^[41], but also influence zeolite morphology^[42]. TEAOH (tetraethylammonium hydroxide) is widely used as the template for synthesizing MOR^[43]. At the low concentration of TEAOH (Figures 3B and 4C), MOR microsphere is generated with $\text{SiO}_2/\text{Na}_2\text{O}/\text{H}_2\text{O}/\text{TEAOH}/\text{Al}_2\text{O}_3 = 15/8.3/900/2/1$, in which the TEAOH amount is decreased along with the enhancement of Na_2O for keeping the constant pH value of gels.

In addition, MOR zeolite can be synthesized without TEAOH using the present acidic hydrolysis route. Figure 3B plots the XRD patterns of MOR zeolites obtained with various initial gel compositions in the absence of TEAOH. All the template-free synthesized samples present well defined MOR structures. The SEM image (Figure 4D) shows that the sample Entry 12 is consisted of cylinder-shaped particles sized ca. $40 \mu\text{m}$, and these micron-sized particles are assembled by the fibrous small-sized crystals, similar to that reported by Zhang *et al.*^[39]. It is interesting to find that several morphologies of mordenite crystals, such as elongated spindle (Entry 13, Figure 4E), short spindle (Entry 14, Figure 4F), petal (Entry 15, Figure 4G) and circular pie (Entry 16, Figure 4H), can be obtained by varying synthetic factors in the absence of template agent. Among them, the petal-like morphology has never been reported. However, bulky spheres can not be obtained in the absence of TEAOH. Figure S8c-g illustrates the nitrogen sorption isotherms of these template-free samples, giving distinct nitrogen uptakes at low relative pressures ($p/p_0 < 0.1$), and Table S1 shows considerable surface areas of 232 - $338 \text{ m}^2 \text{ g}^{-1}$ and pore volumes of 0.12 - $0.18 \text{ cm}^3 \text{ g}^{-1}$, lower than those of the samples with TEAOH. This indicates that the synthesis conditions may be further modified (e.g., longer crystallization time) to improve the quality of the template-free MOR phase.

4. Discussion

Various MOR zeolites with controlled morphologies can be synthesized through the hydrothermal route involving the acidic hydrolysis of TEOS. Scheme 1 demonstrates the variation and evolution of MOR morphologies with the different synthetic conditions. The unusual micron-sized bulky spherical mordenite ($40 \mu\text{m}$) is synthesized with low initial $\text{SiO}_2/\text{Al}_2\text{O}_3$ and $\text{Na}_2\text{O}/\text{Al}_2\text{O}_3$ ratios in relative diluted solution. With the raise of $\text{SiO}_2/\text{Al}_2\text{O}_3$ ratio, the shape of crystal aggregates change from bulky spheres (Entry 1, Figure 2A) to circular pies (Entry 2, Figure 2B), and then to flat prisms (Entry 3, Figure 2C). Also, with higher $\text{Na}_2\text{O}/\text{Al}_2\text{O}_3$ ratio, the MOR crystal changes from microsphere (Entry 1) to circular pie (Entry 4). The morphology of the sample Entry 4 (Figure 2D) is similar to Entry 2 (Figure 2B), but the primary particle of the former is more fused than the later. When the temperature increases to 473 K (Entry 8), hexagonal star-like prism appears (Figure 2J), which has never been reported as far as we know. Nonetheless, detailed formation



Scheme 1. The evolution of mordenite morphologies with the different synthetic conditions.

mechanism is not clear and needs further investigation. For the synthesis of the bulky spheres, TEOAH not only plays a template role in growing zeolite MOR but also is crucial for assembling spheres, as the same synthesis process without using TEOAH fails to generate bulky spheres. Besides, diluting the synthesis gel by adding more water causes the change of morphology from circular pie (Entry 9) to ellipsoid (Entry 10), and finally to bulky sphere (Entry 1).

Previously, aggregation-densification-zeolitization mechanism explained the formation of the spherical aggregates of zeolites^[44]. At early crystallization stage, amorphous aluminosilicate particles are created from the Si and Al species via the formation of Si–O–Al bonds^[45], with one amorphous particle containing one nucleus of zeolite crystal^[46]. These amorphous particles are gradually gathered to form the inorganic-organic composites under the attraction of TEOAH as a splice agent. As the crystallization time is prolonged, these composites grow bigger by wrapping the amorphous particles around them^[8], and then the nuclei rapidly grow into numerous crystals until the surrounding nutrients are consumed^[26]. It is suggested that amorphous silicates should favor the formation of small-sized crystals because the amount of nutrients around nuclei is quite limited^[28]. Along with this process, the small-sized crystals have the tendency to aggregate into micron-sized spheres in order to lower the surface potential^[46, 47]. Besides, the vigorous stirring during the nucleation process also benefits the formation of spherical secondary particles due to the influence of shearing force field^[48]. Owing to these factors, the spheres assembled by small-sized crystals can be achieved with the acidic hydrolysis route by controlling the elemental synthetic conditions.

5. Conclusions

In summary, three unusual morphologies of bulky sphere, petal hexagonal prism and petal for mordenite zeolite (MOR) are synthesized with the hydrothermal approach involving the acidic hydrolysis of tetraethylorthosilicate. Using tetraethylammonium hydroxide as the template, the morphology of MOR zeolite can be changed to circular pie, flat prism, hexagonal star-like prism, ellipsoid, *etc.* Besides, versatile morphologies can be also

adjusted in template-free synthesis pathway. During the synthesis, the morphology control is achieved simply through tuning the elemental synthetic conditions, therefore providing a facile way for the morphology-controlled synthesis of MOR zeolite.

Acknowledgements

The authors thank the National Natural Science Foundation of China (Nos. 20976084, 21136005 and 21303038) and Jiangsu Province Science Foundation for Youths (No. BK20130921).

Notes and references

State Key Laboratory of Materials-Oriented Chemical Engineering, College of Chemistry and Chemical Engineering, Nanjing Tech University, Nanjing 210009, Jiangsu, P. R. China

*Corresponding author, E-mail: junwang@njtech.edu.cn, Tel: (+86) 25-83172264

- [1] R. M. Barrer, *Hydrothermal Chemistry of Zeolites*, Academic Press, London, 1982.
- [2] A. Corma, *Chem. Rev.*, 1995, 95, 559-614.
- [3] J. D. Sherman, *Proc. Natl. Acad. Sci.*, 1996, 96, 3471-3478.
- [4] L. Y. Hu, Z. K. Zhang, S. J. Xie, S. L. Liu and L. Y. Xu, *Catal. Commun.*, 2009, 10, 900-904.
- [5] P. Sharma, W. J. Chung, *Desalination*, 2011, 275, 172-180.
- [6] Y. R. Ma, L. M. Qi, J. M. Ma, Y. Q. Wu, O. Liu and H. M. Cheng, *Colloids Surf. A*, 2003, 229, 1-8.
- [7] H. H. Wan, L. Liu, C. M. Li, X. Y. Xue and X. M. Liang, *J. Colloid Interface Sci.*, 2009, 337, 420-426.
- [8] W. G. Lin, M. M. Wan, Y. Zhou, H. C. Gu, S. L. Zhou and J. H. Zhu, *J. Mater. Chem. A*, 2013, 1, 6849-6857.
- [9] Z. P. Huo, X. Y. Xu and J. Q. Song, *Micropor. Mesopor. Mater.*, 2012, 158, 137-140.
- [10] L. Zhang, S. J. Xie, W. J. Xin, X. J. Li, S. L. Liu and L. Y. Xu, *Mater. Res. Bull.*, 2011, 46, 894-900.
- [11] J. Bronic, A. Palcic, B. Subotic and V. Valtchev, *Mater. Chem. Phys.*, 2012, 132, 973-976.
- [12] L. Benco, T. Bucko and J. Hafner, *J. Catal.*, 2011, 277, 104-

- 116.
- [13] K. Y. Leng, S. N. Sun, B. T. Wang, L. Sun, W. Xu and Y. Y. Sun, *Catal. Commun.*, 2012, 28, 64–68.
- [14] K. Y. Leng, Y. Wang, C. M. Hou, C. Lancelot, C. Lamonier, A. Rives and Y. Y. Sun, *J. Catal.*, 2013, 306, 100–108.
- [15] H. How, *J. Chem. Soc.*, 1864, 17, 100-104.
- [16] W. M. Meier, *Zeitschrift für Kristallographie.*, 1961, 115, 439-450.
- [17] S. V. Donk, J. H. Bitter, A. Verberckmoes, M. Versluijs-Helder, A. Broersma and K. P. de Jong, *Angew. Chem. Int. Ed.*, 2005, 44, 1360-1363.
- [18] P. Sharma, P. Rajaramb and R. Tomar, *J. Colloid Interface Sci.*, 2008, 325, 547-557.
- [19] R. F. Zhou, Z. L. Hu, N. Hu, L. Q. Duan, X. S. Chen and H. Kita, *Micropor. Mesopor. Mater.*, 2012, 156, 166-170.
- [20] G. Ertl, J. Weitkamp, *Preparation of Solid Catalysis*, Wiley-VCH, Weinheim, 1999, pp. 4.
- [21] M. Matsui, Y. Kiyozumi, T. Yamamoto, Y. Mizushina, F. Mizukami and K. Sakaguchi, *Chem. Eur. J.*, 2001, 7, 1555-1560.
- [22] F. Xu, Y. J. Wang, X. D. Wang, Y. H. Zhang, Y. Tang and P. Y. Yang, *Adv. Mater.*, 2003, 15, 1751-1753.
- [23] Y. J. Kang, W. Shan, J. Y. Wu, Y. H. Zhang, X. Y. Wang, W. L. Yan and Y. Tang, *Chem. Mater.*, 2006, 18, 1861-1866.
- [24] R. M. Mohamed, H. M. Aly, M. F. El-Shahat and I. A. Ibrahim, *Micropor. Mesopor. Mater.*, 2005, 79, 7-12.
- [25] B. Tan, S.E. Rankin, *J. Phys. Chem. B*, 2006, 110, 22353-22364.
- [26] J. Gu, Y. J. Wu, J. Wang, Y. D. Lu and X. Q. Ren, *J. Mater. Sci.* 2009, 44, 3777-3783.
- [27] Y. J. Wu, X. Q. Ren and J. Wang, *Mater. Chem. Phys.*, 2009, 113, 773-779
- [28] F. F. Cao, Y. J. Wu, J. Gu and J. Wang, *Mater. Chem. Phys.*, 2011, 130, 727-732.
- [29] Y. J. Wu, J. Wang, *J. Am. Chem. Soc.*, 2010, 132, 17989-17991.
- [30] B. O. Hincapie, L. J. Garces, Q. Zhang, A. Sacco and S. L. Suib, *Micropor. Mesopor. Mater.*, 2004, 67, 19–26.
- [31] S. Mintova, V. Valtchev, T. Onfroy, C. Marichal, H. Knozinger and T. Bein, *Micropor. Mesopor. Mater.*, 2006, 90, 237-245.
- [32] C. J. Brinker, G. W. Scherer, *J. Non-Cryst. Solids*, 1985, 70, 301-322.
- [33] J. Sanchez, A. McCormick, *J. Phys. Chem.*, 1992, 96, 8973-8979.
- [34] J. Sefcik, A.V. McCormick, *Catal. Today*, 1997, 35, 205 - 223.
- [35] Y. S. Ko, W. S. Ahn, *Powder Technol.*, 2004, 145, 10-19
- [36] R.W. Thompson, *Mol. Sieves*, 1998, 1, 1-31.
- [37] P. Phiriyawirut, R. Magaraphan, A. M. Jamieson and S. Wongkasemjit, *Mater. Sci. Eng. A*, 2003, 361, 147-154.
- [38] K. Suzuki, Y. Kiyozumi, K. Matsuzaki and S. Shin, *Appl. Catal.*, 1987, 35, 401-409.
- [39] L. Zhang , A. N. C. V. Laak, P. E. D. Jongh and K. P. D. Jong, *Micropor. Mesopor. Mater.*, 2009, 126, 115-124.
- [40] O. A. Fouad, R. M. Mohamed, M. S. Hassan and I. A. Ibrahim, *Catal. Today*, 2006, 116, 82-87
- [41] B. M. Lok, T. R. Cannan and C. A. Messina, *Zeolites*, 1983, 3, 282-291.
- [42] L. H. Ding, Y. Zheng, *Mater. Res. Bull.* 2007, 42, 584-590.
- [43] T. Selvam, W. Schwieger, *Stud. Surf. Sci. Catal.*, 2002, 42, 407–414.
- [44] D. P. Serrano, M. A. Uguina, R. Sanz and E. Castillo, *Micropor. Mesopor. Mater.*, 2004, 69, 197-208.
- [45] G. Harvey, L. S. D. Glasser, *ACS Symp. Ser.*, 1989, 398, 49-65.
- [46] S. Mintova, N. H. Olson and T. Bein, *Angew. Chem. Int. Ed.*, 1999, 38, 3201-3204.
- [47] Y. Zhou, W. G. Lin, J. Yang, L. Gao, N. Lin, J. Y. Yang, Q. Hou, Y. Wang and J. H. Zhu, *J. Colloid. Interface. Sci.*, 2011, 364, 594-604.
- [48] C. Z. Yu, J. Fan, B. Z. Tian and D. Y. Zhao, *Chem. Mater.*, 2004, 16, 889-898.